29 January 1999

ELSEVIER

Chemical Physics Letters 300 (1999) 207–212

CHEMICAL PHYSICS LETTERS

The OH production from the $\pi-\pi^*$ transition of acetylacetone

Min-Chul Yoon, Young S. Choi, Sang Kyu Kim *

Department of Chemistry, Inha University, Inchon 402-751, South Korea

Received 16 September 1998; in final form 19 November 1998

Abstract

Acetylacetone in its enolic form has been found to produce the OH radical as a photofragment after the $\pi-\pi^*$ transition induced by UV irradiation. The absorption spectrum of the enolic acetylacetone in the supersonic jet, deduced from the OH photofragment excitation spectrum, shows no distinct structures suggesting the very fast decay of the S_1 state being followed by the C–O chemical bond dissociation. The photodissociation mechanism is discussed with a qualitative description of the energetics involved.

1. Introduction

The acetylacetone molecule forms versatile and useful chelate compounds with various kinds of metals, and therefore its structure and reactivity have been important issues in many fields of science [1–5]. Acetylacetone has two interesting structural isomers, diketo and enol, and it is well known from spectroscopic evidences that the relative population of these two varies depending on the characteristics of environment [6,7]. For instance, the diketo and enol forms are favored in polar and non-polar solvents, respectively, while the enol form is predominant in the gas phase at room temperature [6,7]. The enol form of acetylacetone is stabilized via a strong intramolecular hydrogen bonding in its cyclic conjugated system, of which the stabilization energy has been theoretically predicted to be ~ 12 kcal/mol [8]. The structure of the enolic acetylacetone in the ground electronic state has been intensively studied but still seems to remain controversial in terms of whether it belongs to C_{2v} or C_s [9–13]. The intramolecular proton transfer dynamics of the enolic acetylacetone have also been both experimentally and theoretically studied due to its interesting cyclic structure [14–17].

In contrast to the extensive studies on the molecular structure and proton transfer dynamics of acetylacetone, its photochemistry has received relatively less attention. The UV absorption spectrum of acetylacetone in the gas phase at room temperature shows a very broad structureless band, which starts at ~ 313 nm and peaks at ~ 270 nm being ascribed to the spin-allowed $\pi-\pi^*$ transition of the enolic acetylacetone [7]. Later, the similar absorption feature was also found in the electron-impact spectroscopic study by Kuppermann and coworkers [18]. More recently, Roubin et al. has reported the UV-induced isomerization of acetylacetone in Xe matrices using FT-IR spectroscopy [19]. When the sample was placed un-

* Corresponding author. Fax: +82 32 867 5604; e-mail: skkim@inha.ac.kr

0009-2614/99/$ - see front matter
PII: S0009-2614(98)01373-6

der broad-band UV light, a large blue shift of the OH vibrational frequency, resulting from the hydrogen-bond breakage, was observed, and this was attributed to the UV-induced isomerization of the enolic acetylacetone. They could not observe any evidence of the chemical bond cleavage of the molecule and concluded that the only process involved in the $(\pi-\pi^*)$ state decay in the matrix environment is the stereoisomerization [19].

Here, we prepared acetylacetone in a supersonic jet and induced the $\pi-\pi^*$ transition by the nanosecond laser pulse. In a collisionless condition, we could easily detect the prompt production of the OH radical as a result of photodissociation. This fact indicates that the decay of the $(\pi-\pi^*)$ state is followed by the chemical bond dissociation to give the OH fragment, suggesting that the isomerization is not the only process involved in the $(\pi-\pi^*)$ state decay at least in the gas phase.

2. Experimental

Acetylacetone (Aldrich, 99 + %) was purchased and used without further purification. The sample was kept at room temperature, and the He carrier gas was bubbled through the sample. The gas mixture was then expanded into a vacuum chamber through a 0.5 mm diameter nozzle orifice (General Valve Series 9) with a typical backing pressure of 1 atm. The nozzle was operated with a repetition rate of 10 Hz by a home-made nozzle-driver, and it was heated to 70°C to reduce the cluster formation. The vacuum chamber was equipped with a 6-in. diffusion pump and liquid N_2 trap. The background pressure was maintained below $\sim 10^{-5}$ Torr when the nozzle was on.

The second harmonic output of the Nd:YAG laser (Spectra-Physics GCR-150, 7 ns duration) was split in half and used for pumping two independent dye lasers. One dye laser (Lumonics, HD-500) was used to generate the laser pulse in the 560–620 nm range, of which the frequency was doubled by using a KD*P crystal in the autotracker to give the UV laser pulse in the 280–310 nm range. The other dye laser (Lamda-Physik, Scanmate II) was used to generate the laser pulse in the 560–575 nm range. The frequency was also doubled to give the UV laser pulse covering the 280–287 nm range. The former was used to excite the parent molecule (the pump laser pulse), and the latter was used to probe the OH product (the probe laser pulse). For measurement of the laser-induced fluorescence (LIF) of OH, the fourth harmonic output (266 nm) of the Nd:YAG laser was also used for the pump. For measurement of the photofragment excitation (PHOFEX) spectra, the pump laser wavelength was scanned while the probe laser frequency was fixed to monitor the LIF signal of the specific quantum state of OH.

The pump and probe laser pulses were combined with a dichroic mirror, directed into the chamber collinearly, and overlapped with a supersonic beam at the position of ~ 20 mm downstream from the nozzle orifice. The polarizations of two pulses were perpendicular to each other, and the polarization of the pump laser pulse was perpendicular to the direction of the fluorescence detection. The laser intensity variation with a wavelength scan was monitored by a photodiode and normalized in the process of data analysis. The LIF signal was detected by a PMT (Hamamatsu, H-1949-50), averaged by a integrated boxcar (SRS, SR250), A/D converted by a interface (SRS, SR245), and stored in a personal computer by a data-taking program which also controlled two dye lasers and crystal autotrackers. The intensity of the probe laser was reduced so that the OH transition is not saturated. The linearity of the LIF signal with the probe laser intensity was carefully checked.

3. Results and discussion

A typical laser-induced fluorescence (LIF) spectrum of the nascent OH product from the photodissociation of acetylacetone at 266 nm is shown with partial assignments [20] in Fig. 1. The $A^2\Sigma^+$ $(v=1)$–$X^2\Pi$ $(v=0)$ transition of OH is used for the LIF measurement. In Fig. 2, the OH rotational state distributions at photolysis wavelengths of 291 and 266 nm, deduced from LIF intensities of R_1 branches divided by adequate values of Einstein coefficients [21], are shown with corresponding Boltzmann plots. The rotational state distribution is peaked at $N=3$ at 291 nm and $N=4$ at 266 nm, and the average rotational energies are calculated to be 470 and 540 cm^{-1} at 291 and 266 nm, respectively. Here, the

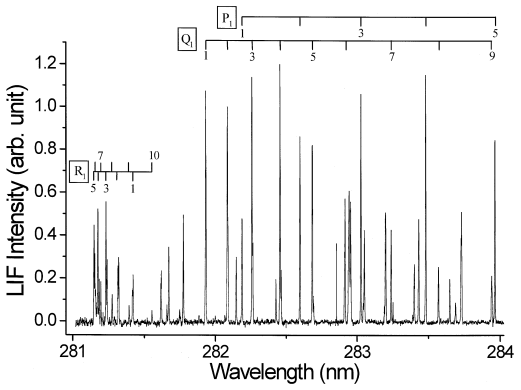

Fig. 1. A typical LIF spectrum of the OH fragment using the $A^2\Sigma^+$ ($v=1$)–$X^2\Pi$ ($v=0$) transition. The pump wavelength is 266 nm. Assignments of the peaks are from Ref. [20].

rotational energies at both photolysis energies are averaged using population distributions normalized over the $N=1\sim10$ range. Thus, it should be noted that the OH rotational energies are slightly underestimated here since rotational states with $N>10$ are also found to be populated specially at 266 nm, although their contribution is not considerably large. The Boltzmann plots give the rotational temperatures of the nascent OH fragments of 540 and 630 K at 291 and 266 nm, respectively. The uncertainties of the rotational temperatures are within $\pm20\%$. No vibrationally excited OH is detected even at the pump wavelength of 266 nm. Here, only single spin–orbit state of OH is used for the relative population measurement. A further detailed analysis of the OH rotational state distribution including the relative population of spin–orbit states will be given elsewhere, since it may distract our main point here, which is the fact that the major decay channel of the excited (π–π^*) state is not just the stereoisomerization but the chemical bond dissociation to give the OH fragment.

In Fig. 3, the photofragment excitation (PHOFEX) spectra are shown. In Fig. 3a, the LIF intensity from the $P_1(4)$ level of OH is monitored as a function of the photolysis energy. The time delay between the pump and probe laser pulses is fixed at 40 ns. The OH LIF signal increases smoothly with increasing the photolysis energy without any distinct structures. In order to enhance the signal/noise ratio, the pump laser pulse is mildly focused onto the molecular beam for the $P_1(2)$ PHOFEX spectrum taken at $\Delta t=$ 10 ns (Fig. 3b). Many sharp peaks observed in the 306–310 nm range are found to represent LIF signals due to $A^2\Sigma^+$ ($v=0$)–$X^2\Pi$ ($v=0$) transitions of OH product [20], induced by the two photon process of the focused pump laser pulse only; one photon pumps the enolic acetylacetone molecule and the other photon probes the OH product within its pulse duration of 7 ns. Since there is no sharp rise of the signal in the PHOFEX spectrum, it is non-trivial to determine the threshold energy for the OH detection accurately. Thus, only the upper bound of the threshold energy for the OH detection could be roughly estimated to be around 92 kcal/mol, which corresponds to 312 nm in the PHOFEX spectrum (Fig. 3b). The PHOFEX spectra for different OH rotational transitions such as $Q_1(4)$ and $Q_1(3)$ are

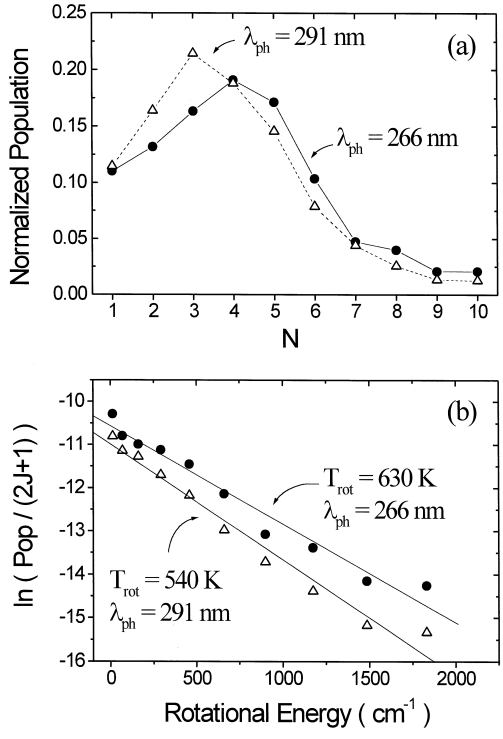

Fig. 2. (a) The OH ($v=0$) rotational state distribution from the photolysis of the enolic acetylacetone at 291 and 266 nm, (b) Boltzmann Plots giving the rotational temperatures of 540 K at 291 nm and 630 K at 266 nm. Uncertainties are within $\pm20\%$. In (a), lines connecting data points are drawn just for the visual aid.

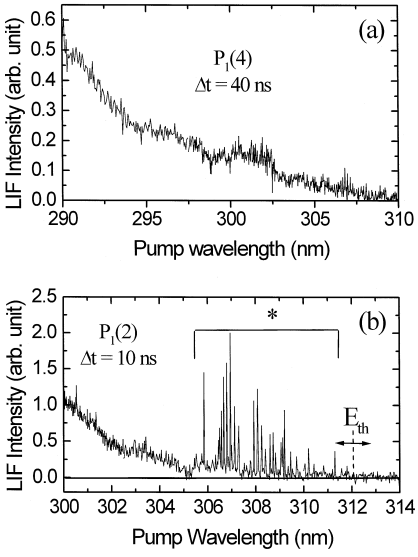

Fig. 3. PHOFEX spectra monitoring (a) the $P_1(4)$ line intensity at $\Delta t = 40$ ns and (b) the $P_1(2)$ line intensity at $\Delta t = 10$ ns as a function of the pump wavelength. In (b), sharp peaks noted as an asterisk are due to the $A^2\Sigma^+$ $(v = 0)$–$X^2\Pi$ $(v = 0)$ transitions [20], which are originated from the two photon process of the pump laser only (see the text).

found to be almost identical to those shown in Fig. 3. The PHOFEX spectra taken at the time delay of 10 ns show little difference in the absolute LIF intensity from those taken at 40 ns, which suggests that the rate constant for the OH appearance is comparable or larger than 10^8 s^{-1} at least within the energy range carried out in this work. The wavelength of 312 nm, estimated from the threshold energy of PHOFEX spectra, is very close to the origin of the π–π^* transition measured in the gas-phase absorption spectrum at room temperature [7]. Therefore, the PHOFEX spectrum could be a good representation of the absorption spectrum of the enolic acetylacetone in the cold jet, although the changes of the OH rotational state distribution and the reaction rate with increasing the pump energy might affect the detailed shape of the PHOFEX spectrum [22]. As shown in Fig. 3, no distinct structures are observed in the PHOFEX spectra even at the energy region near the origin, which suggests that the broadness of the π–π^* absorption may be due to the very short lifetime of the excited state. No fluorescence has been observed from the π–π^* state, and this is also consistent with above. Therefore, one can imagine that the π–π^* state is followed by very fast non-radiative decay processes, and they could be internal conversion to the ground state or intersystem crossing to the lowest triplet state.

The upper bound of the available energy for the OH fragment could be roughly estimated from the highest rotational quantum number detectable in the LIF spectrum taken at the photolysis energy of 297.5 nm (96.1 kcal/mol). The highest rotational quantum number giving the detectable LIF signal is $N = 10$, of which the rotational energy is 5.8 kcal/mol. Therefore, the bond dissociation energy should be less than $96.1–5.8 = 90.3$ kcal/mol. As a cross-check, the highest N value in the OH LIF spectrum taken at 266 nm (107.5 kcal/mol) is investigated to give $N = 17$, of which the corresponding rotational energy is 15.7 kcal/mol. This gives 91.8 kcal/mol for the upper bound of the OH production threshold energy, which is not far away from the above estimated value. If the stabilization energy of intramolecular hydrogen bonding is taken to be 12 kcal/mol [8], then the C–OH bond dissociation energy would be $90.3–12 = 78.3$ kcal/mol, which is not an unreasonable value for the C–O bond energy. Suppose that this energetics is correct, then the fraction of the available energy transferred to the OH rotational energy (vide supra) is calculated to be $\sim 16\%$ at 291 nm ($E_{rot} = 1.3$ kcal/mol out of $E_{avl} = 98.2–90.3 = 8$ kcal/mol) and $\sim 9\%$ at 266 nm ($E_{rot} = 1.53$ kcal/mol out of $E_{avl} = 107.5–90.3 = 17.2$ kcal/mol).

If the excited molecule undergoes the internal conversion to the highly vibrationally excited state and a complete randomization among all the energetically available states occurs before the dissociation, then the statistical partitioning of the available energy is expected. In this case, the OH rotational energy would be just around 5% of the total available energy, since the molecular size is big (the total number of normal modes $= 39$) and only two modes contribute to the OH rotation in the fragmentation process. That is, the statistical model predicts a much smaller percentage for the partitioning to the rotational degree of freedom than experimental values of $9 \sim 16\%$ observed here. Thus especially at the energy near the threshold region where the partition to the rotational energy is comparable or more than

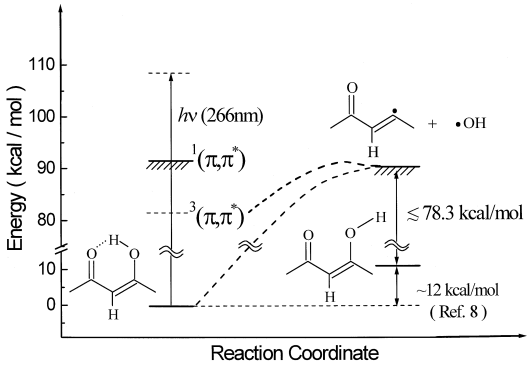

Fig. 4. A schematic diagram showing the energetics involved in the photodissociation of the enolic acetylacetone. The upper bounds of the $\pi-\pi^*$ origin and the bond dissociation energy are shown with hatched lines.

16%, the reaction coordinate may be strongly coupled to the H–O–C bending or torsional motion about the breaking C–O bond, inducing both the breakage of the hydrogen-bonding and the non-statistical release of the available energy to the OH rotational degree of freedom. Accordingly, the dissociation may experience a small exit barrier, of which the impulsive nature along the reaction coordinate where bending or torsional motions are strongly coupled, giving the more rotational energy to the OH product than the statistical model predicts. It should be noted however that, as pointed out in many studies [23–25], as the energy increases above the reaction barrier, the impulsive nature becomes less important, while the statistical nature comes in to play an important role in partitioning of the available energy into the various degrees of freedom of fragments. Therefore, the average rotational energy would have the less portion at the higher photolysis energy, which is consistent with our finding that the rotational fraction is 9% of the total available energy at 266 nm, while it is 16% at 291 nm.

It is not certain right now which electronic states are involved in the chemical bond dissociation. However, one can imagine the exit barrier induced by the avoided crossing of the lowest triplet $^3(\pi-\pi^*)$ state and a dissociative upper state containing the σ^* character along the C–OH bond (Fig. 4). For the better understanding of the photodissociation pathway, theoretical calculations on the potential energy surfaces along the reaction coordinate should be carried out along with more experimental works such as studies of Doppler profiles and vector correlation.

4. Conclusions

Here, we have found that the enolic acetylacetone in the gas phase gives rise to the OH fragment upon the $\pi-\pi^*$ transition. No fluorescence has been observed from the $(\pi-\pi^*)$ state of the enolic acetylacetone. The photofragment excitation spectrum shows that there are no sharp structures in the absorption even in the cold jet, suggesting the ultrashort lifetime of the excited state. The energy release to the OH rotation, and its dependence on the photolysis energy suggests that the C–O–H bending and torsional modes about the dissociating C–O bond may be strongly coupled to the reaction coordinate in the energy range near the $\pi-\pi^*$ origin. The partitioning ratio of the available energy to the OH rotational energy is found to decrease as the available energy increases, demonstrating that as the energy above the barrier increases dynamics of the excited molecule are less influenced by the detailed shape of the potential energy surface in the vicinity of the transition state.

Acknowledgements

We thank to Mrs. Chung-Hyun Lim for her great help in the beginning stage of this work. This work was financially supported by the Korea Science and Engineering Foundation (Project No. 971-0305-037-2) and Inha University (1997).

References

[1] T. Chiavassa, P. Verlaque, L. Pizzala, P. Roubin, Spectrochim. Acta 50A (1994) 343.
[2] G.S. Hammond, W.G. Borduin, G.A. Guter, J. Am. Chem. Soc. 81 (1959) 4682.
[3] B. Bock, K. Flatau, H. Junge, M. Kuhr, H. Musso, Angew. Chem. Int. Ed. Engl. 10 (1971) 225.
[4] M.S. Gordon, R.D. Koob, J. Am. Chem. Soc. 95 (1973) 5863.
[5] R.H. Holm, F.A. Cotton, J. Am. Chem. Soc. 80 (1958) 5658.
[6] J. Powling, H.J. Bernstein, J. Am. Chem. Soc. 73 (1951) 4553.

[7] H. Nakanishi, H. Morita, S. Nagakura, Bull. Chem. Soc. Jpn 50 (1977) 2255.
[8] J.J. Dannenberg, R. Rios, J. Phys. Chem. 98 (1994) 6714.
[9] A.H. Lowrey, C. George, P. D'Antonio, J. Karle, J. Am. Chem. Soc. 93 (1971) 6399.
[10] K. Iijima, A. Ohnogi, S. Shibata, J. Mol. Struct. 156 (1987) 111.
[11] N.S. Hush, M.K. Livett, J.B. Peel, G.D. Willett, Aust. J. Chem. 40 (1987) 599.
[12] R.S. Brown, J. Am. Chem. Soc. 99 (1977) 5497.
[13] A.D. Isaacson, K. Morokuma, J. Am. Chem. Soc. 97 (1975) 4453.
[14] C. Choi, M.M. Pintar, J. Chem. Phys. 106 (1977) 3473.
[15] G. Karlström, B. Jönssen, B. Roos, H. Wennerström, J. Am. Chem. Soc. 98 (1976) 6851.
[16] X. Krokidis, V. Goncalves, A. Savin, B. Silvi, J. Phys. Chem. A 102 (1998) 5065.
[17] K. Hinsen, B. Roux, J. Chem. Phys. 106 (1997) 3567.
[18] K.N. Walzl, I.M. Xavier Jr., A. Kuppermann, J. Chem. Phys. 86 (1987) 6701.
[19] P. Roubin, T. Chiavassa, P. Verlaque, I. Pizzala, H. Bodot, Chem. Phys. Lett. 175 (1990) 655.
[20] G.H. Dieke, H.M. Crosswhite, J. Quantum Spectrosc. Radiat. Transfer 2 (1962) 97.
[21] I.L. Chidsey, D.R. Crosley, J. Quantum Spectrosc. Radiat. Transfer 23 (1980) 187.
[22] S.K. Kim, E.R. Lovejoy, C.B. Moore, J. Chem. Phys. 102 (1995) 3202.
[23] S.W. North, D.A. Blank, J.D. Gezelter, C.A. Longfellow, Y.T. Lee, J. Chem. Phys. 102 (1995) 4447.
[24] W.H. Green, C.B. Moore, W.F. Polik, Annu. Rev. Phys. Chem. 43 (1992) 591.
[25] A.H. Zewail, Femtochemistry: Ultrafast Dynamics of the Chemical Bond, World Scientific, Singapore, 1994.